

Underscreened Kondo effect in quantum dots coupled to ferromagnetic leads

Ireneusz Weymann^{1,2,*} and László Borda^{3,4}

¹*Department of Physics, Adam Mickiewicz University, 61-614 Poznań, Poland*

²*Physics Department, Arnold Sommerfeld Center for Theoretical Physics and Center for NanoScience, Ludwig-Maximilians-Universität, Theresienstrasse 37, D-80333 Munich, Germany*

³*Department of Theoretical Physics and Research Group “Physics of Condensed Matter” of the Hungarian Academy of Sciences, Budapest University of Technology and Economics, Budafoki út 8., H1111 Budapest, Hungary*

⁴*Physikalisches Institut and Bethe Center for Theoretical Physics, Universität Bonn, Nussallee 12, D-53115 Bonn, Germany*

(Dated: November 7, 2018)

We analyze the equilibrium transport properties of underscreened Kondo effect in the case of a two-level quantum dot coupled to ferromagnetic leads. Using the numerical renormalization group (NRG) method, we have determined the gate voltage dependence of the dot’s spin and level-resolved spectral functions. We have shown that the polarization of the dot is very susceptible to spin imbalance in the leads and changes sign in the middle of the $S = 1$ Coulomb valley. Furthermore, we have also found that by fine-tuning an external magnetic field one can compensate for the presence of ferromagnetic leads and restore the Kondo effect in the case of $S = \frac{1}{2}$ Coulomb valley. However, the underscreened Kondo effect cannot be fully recovered due to its extreme sensitivity with respect to the magnetic field.

PACS numbers: 72.25.-b, 73.63.Kv, 85.75.-d, 72.15.Qm

I. INTRODUCTION

Ever since the observation of the resistivity anomaly in normal metals at low temperatures,¹ the Kondo problem² has been investigated perpetually both experimentally and theoretically.^{3–5} As a result of that intensive research, in many respects, the Kondo effect is well understood now. Very recently the interplay between the Kondo effect and other many-body phenomena, such as superconductivity or ferromagnetism, has attracted a lot of interest. That attention was mainly motivated by the recent advances in nanofabrication which have opened the possibility to attach superconducting^{6,7} or ferromagnetic^{8–13} leads to molecules or semiconducting quantum dots. In the following we will focus our attention on the case of ferromagnetic leads coupled to a quantum dot exhibiting the Kondo effect.

From the theoretical side, a consensus was found that single level quantum dots (i.e. relatively small dots with level spacing δ larger than the hybridization Γ) attached to ferromagnetic leads exhibit finite spin asymmetry as a result of the spin imbalance in the leads, which gives rise to a splitting and suppression of the Kondo resonance.^{14–17} This spin asymmetry can, however, be compensated by means of an external magnetic field or by tuning the gate voltage properly.^{18,19} In that way the strong coupling Kondo fixed point can be reached, with a fully developed Kondo resonance and a somewhat reduced Kondo temperature. This expectation has recently been confirmed experimentally.^{8–13}

While in many cases the quantum dots can successfully be modelled by only a single local level, there are few exceptions when the finite level spacing affects the low energy physics of such a device considerably. An isolated quantum dot with even number of electrons can

have spin triplet $S = 1$ ground state, if the level spacing between the two single particle levels closest to the Fermi energy is anomalously small, i.e. smaller than the exchange coupling between the two electrons situated on those levels. If such a device is attached to only one lead then the system will exhibit the so-called *underscreened* Kondo effect.^{20–24} A single lead can only screen half of the local spin below the Kondo temperature T_K while the residual spin-a-half object is left unscreened with a ferromagnetic Kondo coupling to the rest of the conduction electrons. Such a ferromagnetic Kondo coupling is known to be irrelevant in renormalization group sense, as it scales to zero when the energy scale is lowered, resulting in a Fermi liquid plus a decoupled $S = \frac{1}{2}$ object at zero temperature. This behavior is reached in a non-analytic fashion resulting in singular terms in e.g. the single particle scattering rate. Such kind of behavior was recently termed as *singular Fermi liquid*.^{22,24}

In a real quantum dot subject to a transport experiment the situation is slightly more complex as the dot has to be coupled to two leads to drive current through it. Even if the second lead is just a weakly coupled probe, its presence introduces a second energy scale, $T'_K \ll T_K$, at which the residual spin-a-half is screened by the other lead mode. The screening takes place in two stages and the separation between the energy scales T_K and T'_K can be tuned by the asymmetry between the coupling to the leads. Since the Kondo temperature is exponentially sensitive to the coupling, a realistic value of asymmetry is enough to separate the two stages completely. In such a case, if the other experimentally relevant energy scales, such as temperature T or magnetic field B , lie in between the two Kondo temperatures $T'_K \ll B, T < T_K$, then the system is well described by the underscreened Kondo model. In fact, very recently, underscreened Kondo effect

was observed experimentally in molecular quantum dots coupled to nonmagnetic leads.²⁵

In the present paper we focus our interest on the interplay of underscreened Kondo effect and itinerant electron ferromagnetism in the leads. To that end we consider a two level quantum dot coupled to a single reservoir of conduction electrons exhibiting spin imbalance. We assume that the second Kondo temperature is always much smaller than the experimental temperature, therefore we consider the second lead as a weakly coupled probe only.

II. THEORETICAL DESCRIPTION

The considered system consists of a two-level quantum dot coupled to a ferromagnetic reservoir, see Fig. 1, and its Hamiltonian is given by

$$H = H_{\text{FM}} + H_{\text{QD}} + H_{\text{tun}}, \quad (1)$$

where the first term describes the noninteracting itinerant electrons in ferromagnetic lead, $H_{\text{FM}} = \sum_{k\sigma} \varepsilon_{k\sigma} c_{k\sigma}^\dagger c_{k\sigma}$, where $c_{k\sigma}^\dagger$ is the electron creation operator with wave number k and spin σ , while $\varepsilon_{k\sigma}$ is the corresponding energy. The second part of the Hamiltonian describes a two-level quantum dot and is given by

$$H_{\text{QD}} = \sum_{j\sigma} \varepsilon_j d_{j\sigma}^\dagger d_{j\sigma} + U \sum_j n_{j\uparrow} n_{j\downarrow} + U' \sum_{\sigma\sigma'} n_{1\sigma} n_{2\sigma'} + JS^2 + BS^z, \quad (2)$$

where $n_{j\sigma} = d_{j\sigma}^\dagger d_{j\sigma}$ and $d_{j\sigma}^\dagger$ creates a spin- σ electron in the j th level ($j = 1, 2$), ε_j denotes the corresponding energy of an electron in the dot. Here, $\varepsilon_1 = \varepsilon - \delta/2$ and $\varepsilon_2 = \varepsilon + \delta/2$, with $\delta = \varepsilon_2 - \varepsilon_1$ being the level spacing. The on-level (inter-level) Coulomb correlations are denoted by U (U'), respectively. J is the ferromagnetic exchange coupling ($J < 0$) with $\vec{S} = \vec{S}_1 + \vec{S}_2$, where $\vec{S}_j = \frac{1}{2} \sum_{\sigma\sigma'} d_{j\sigma}^\dagger \vec{\sigma}_{\sigma\sigma'} d_{j\sigma'}$ is the spin operator for electrons in the dot level j and $\vec{\sigma}$ denotes the vector of Pauli spin matrices. The last term of H_{QD} describes the Zeeman splitting with B ($g\mu_B \equiv 1$) being the external magnetic field applied along the z th direction.

Finally, the tunnel Hamiltonian is given by

$$H_{\text{tun}} = \sum_{kj\sigma} t_{j\sigma} \left(d_{j\sigma}^\dagger c_{k\sigma} + c_{k\sigma}^\dagger d_{j\sigma} \right), \quad (3)$$

where $t_{j\sigma}$ describes the spin-dependent hopping matrix elements between the j th dot level and ferromagnetic lead. The strength of the coupling between the dot and lead can be expressed as $\Gamma_{j\sigma} = \pi\rho|t_{j\sigma}|^2$, where ρ is the density of states (DOS) in the lead. In the following, we assume a flat band of width $2D$ and use $D \equiv 1$ as energy unit, as not stated otherwise. Note that by assuming constant DOS the whole spin-dependence has been shifted into the coupling constants. While this assumption may simplify the calculations, it does not affect

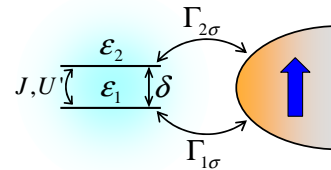


FIG. 1: (color online) Schematic of a two-level quantum dot coupled to a ferromagnetic reservoir with spin polarization p . The dot level energies are denoted by ε_1 and ε_2 , δ is the level spacing, while U' and J describe the inter-level Coulomb correlations and spin exchange interaction. The j th dot level is coupled to ferromagnetic electrode with strength $\Gamma_{j\sigma}$.

the low-energy physics we are interested in.^{16,17} To parameterize the couplings, it is convenient to introduce the spin polarization of ferromagnetic lead, p , defined as $p = (\Gamma_\uparrow - \Gamma_\downarrow)/(\Gamma_\uparrow + \Gamma_\downarrow)$, where we have assumed that each dot level is coupled with the same strength to the lead, $\Gamma_{j\sigma} = \Gamma_\sigma$. Then, the coupling for the spin- \uparrow (spin- \downarrow) electrons can be written as $\Gamma_{\uparrow(\downarrow)} = (1 \pm p)\Gamma$, where $\Gamma = (\Gamma_\uparrow + \Gamma_\downarrow)/2$. For $p = 0$, the couplings do not depend on spin and the system behaves as if coupled to nonmagnetic lead. However, for finite spin polarization, $p \neq 0$, the couplings are spin-dependent, giving rise to an effective exchange field which may spin-split the levels in the dot, suppressing the Kondo resonance. Such behavior has been extensively studied theoretically in the case of single-level quantum dots,^{14–19,26–29} where the usual $S = \frac{1}{2}$ Kondo effect develops, while the effect of ferromagnetism on the other types of Kondo effect remains to a large extent unexplored.

In this paper we thus consider the zero-temperature equilibrium transport properties of two-level quantum dots coupled to ferromagnetic lead in the case of underscreened Kondo effect. In order to perform this analysis in most accurate and exact way, we employ the numerical renormalization group (NRG) method.^{30,31} The NRG consists in a logarithmic discretization of the conduction band and mapping of the system onto a semi-infinite chain with the quantum dot sitting at the end of the chain. By diagonalizing the Hamiltonian at consecutive sites of the chain and storing the eigenvalues and eigenvectors of the system, one can accurately calculate the static and dynamic quantities of the system. In particular, numerical results presented here were obtained using the flexible density-matrix numerical renormalization group (DM-NRG) code, which allows to use arbitrary number of Abelian and non-Abelian symmetries.^{32–34} In fact, exploiting symmetries as much as possible is crucial in obtaining highly accurate data. Because in the case of ferromagnetic leads the full spin rotational invariance is generally broken, in the case of finite spin polarization we have used the Abelian symmetries for the total charge and spin, while in the case of $p = 0$ we have exploited the full spin $SU(2)$ symmetry.

Using the NRG, we have calculated the expecta-

TABLE I: The respective eigenstates $|Q, S^z\rangle$ and eigenvalues E_{Q, S^z} of the decoupled quantum dot Hamiltonian. Here, $Q = (\sum_{j\sigma} n_{j\sigma} - 2)$ and S^z are the charge and z th component of the spin in the dot, while $|\chi_1\chi_2\rangle$ denotes the local states with $\chi_j = 0, \uparrow, \downarrow, d$ for zero, spin-up, spin-down and two electrons in the level j .

n	$ Q, S^z\rangle$	E_{Q, S^z}
1	$ -2, 0\rangle = 00\rangle$	0
2	$ -1, -\frac{1}{2}\rangle = \downarrow 0\rangle$	$\varepsilon - \frac{\delta}{2} + \frac{3J}{4} - \frac{B}{2}$
3	$ -1, -\frac{1}{2}\rangle = 0 \downarrow\rangle$	$\varepsilon + \frac{\delta}{2} + \frac{3J}{4} - \frac{B}{2}$
4	$ -1, \frac{1}{2}\rangle = \uparrow 0\rangle$	$\varepsilon - \frac{\delta}{2} + \frac{3J}{4} + \frac{B}{2}$
5	$ -1, \frac{1}{2}\rangle = 0 \uparrow\rangle$	$\varepsilon + \frac{\delta}{2} + \frac{3J}{4} + \frac{B}{2}$
6	$ 0, 0\rangle = d0\rangle$	$2\varepsilon - \delta + U$
7	$ 0, 0\rangle = 0d\rangle$	$2\varepsilon + \delta + U$
8	$ 0, 0\rangle = \frac{1}{\sqrt{2}}(\uparrow\downarrow\rangle - \downarrow\uparrow\rangle)$	$2\varepsilon + U'$
9	$ 0, -1\rangle = \downarrow\downarrow\rangle$	$2\varepsilon + U' + 2J - B$
10	$ 0, 0\rangle = \frac{1}{\sqrt{2}}(\uparrow\downarrow\rangle + \downarrow\uparrow\rangle)$	$2\varepsilon + U' + 2J$
11	$ 0, 1\rangle = \uparrow\uparrow\rangle$	$2\varepsilon + U' + 2J + B$
12	$ 1, -\frac{1}{2}\rangle = d \downarrow\rangle$	$3\varepsilon - \frac{\delta}{2} + \frac{3J}{4} + U + 2U' - \frac{B}{2}$
13	$ 1, -\frac{1}{2}\rangle = \downarrow d\rangle$	$3\varepsilon + \frac{\delta}{2} + \frac{3J}{4} + U + 2U' - \frac{B}{2}$
14	$ 1, \frac{1}{2}\rangle = d \uparrow\rangle$	$3\varepsilon - \frac{\delta}{2} + \frac{3J}{4} + U + 2U' + \frac{B}{2}$
15	$ 1, \frac{1}{2}\rangle = \uparrow d\rangle$	$3\varepsilon + \frac{\delta}{2} + \frac{3J}{4} + U + 2U' + \frac{B}{2}$
16	$ 2, 0\rangle = dd\rangle$	$4\varepsilon + 2U + 4U'$

tion value of the dot's spin as well as the spectral function of the dot, $A_{jj'\sigma}(\omega) = -\frac{1}{2\pi}\text{Im}[G_{jj'\sigma}^R(\omega) + G_{j'j\sigma}^R(\omega)]$, where $G_{jj'\sigma}^R(\omega)$ denotes the Fourier transform of the dot retarded Green's function, $G_{jj'\sigma}^R(t) = -i\theta(t)\langle\{d_{j\sigma}(t), d_{j'\sigma}^\dagger(0)\}\rangle$. The diagonal elements of the spectral function $A_{j\sigma}(\omega) \equiv A_{jj\sigma}(\omega)$ are related to the spin-resolved density of states, whereas the off-diagonal elements $A_{jj'\sigma}(\omega)$ may be associated with processes of injecting and removing an electron at different sites. The symmetrized spin-resolved spectral function of the dot can be found from

$$A_\sigma(\omega) = \sum_{jj'} A_{jj'\sigma}(\omega). \quad (4)$$

On the other hand, the normalized full spectral function is given by $\pi \sum_\sigma \Gamma_\sigma A_\sigma(\omega)$ and is directly related to the conductivity of the dot.

III. NUMERICAL RESULTS

Before presenting numerical results, it is instructive to analyze the eigen-spectrum of the decoupled quantum dot Hamiltonian, Eq. (2). The respective eigenstates $|Q, S^z\rangle$ and eigenvalues E_{Q, S^z} of H_{QD} are listed in Table I, where $Q = (\sum_{j\sigma} n_{j\sigma} - 2)$ denotes the charge in the dot and S^z is the z th component of the dot spin. By tuning ε the ground state of the dot changes. In particular, in the absence of magnetic field and for ferromagnetic exchange coupling ($J < 0$), when $\varepsilon > \varepsilon_{-2, -1} = \frac{\delta}{2} - \frac{3J}{4}$, the dot is empty, for $\varepsilon = \varepsilon_{-1, 0} = -\frac{\delta}{2} - U' - \frac{5J}{4}$, the doublet $|Q = -1, S = \frac{1}{2}\rangle$ and triplet $|Q = 0, S = 1\rangle$

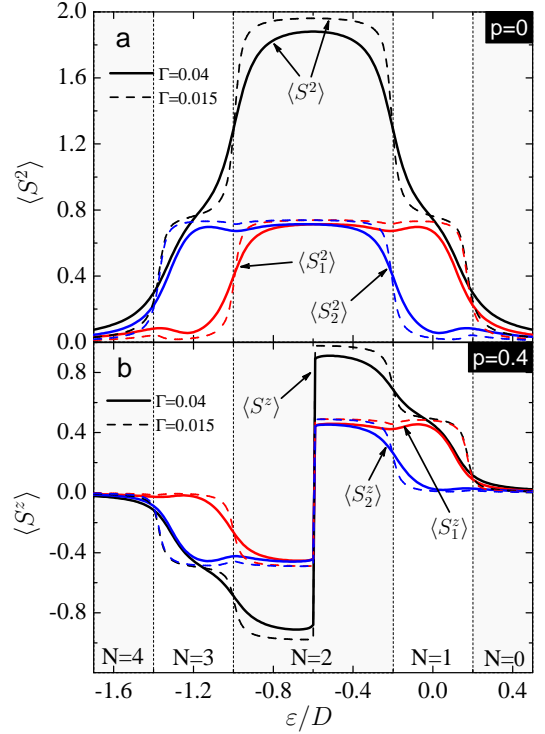


FIG. 2: (color online) The expectation value of the dot spin operator S^2 in presence of nonmagnetic (a) and the expectation value of dot spin operator S^z for ferromagnetic (b) lead as a function of the average level position $\varepsilon = (\varepsilon_1 + \varepsilon_2)/2$. The solid line corresponds to $\Gamma = 0.04$, while the dashed line corresponds to $\Gamma = 0.015$ (in units of $D = 1$). The expectation values separately for the two dot levels are also shown. The parameters are $\delta = 0.1$, $J = -0.2$, $U = U' = 0.4$, $B = 0$, and in the ferromagnetic case $p = 0.4$. The shadowed regions indicate Coulomb valleys with different electron number in the dot, where $N = \sum_{j\sigma} n_{j\sigma}$.

states become degenerate, where now S is the full dot's spin, whereas for $\varepsilon = \varepsilon_{0, 1} = \frac{\delta}{2} - U' - U + \frac{5J}{4}$, the states $|Q = 0, S = 1\rangle$ and $|Q = 1, S = \frac{1}{2}\rangle$ are degenerate. Consequently, for $\varepsilon_{-2, -1} > \varepsilon > \varepsilon_{-1, 0}$, the ground state of the decoupled dot is the doublet and the system will exhibit usual $S = \frac{1}{2}$ Kondo effect, whereas for $\varepsilon_{-1, 0} > \varepsilon > \varepsilon_{0, 1}$ the dot is in the triplet state and the system will show an underscreened Kondo effect. In calculations we have taken the following parameters: $\delta = 0.1$, $J = -0.2$, $U = U' = 0.4$, and $\Gamma = 0.04$ (in units of $D = 1$). One then finds, $\varepsilon_{-2, -1} = 0.2$, $\varepsilon_{-1, 0} = -0.2$ and $\varepsilon_{0, 1} = 1$.

We have calculated the expectation value of the dot's spin operators S^2 and S^z in case of nonmagnetic and ferromagnetic leads, respectively. The results are summarized in Fig. 2. As the level position is lowered by sweeping the gate voltage, the dot is tuned through the Coulomb blockade valleys with electron number $N = 1, 2, 3$ and spin states $S = 1/2, 1, 1/2$, respectively. When the dot is attached to a ferromagnetic lead, the spin asymmetry in the hybridization results in the spin splitting of the dot level, thus leading to a spin polarized

ground state. Precisely in the middle of the $N = 2$ Coulomb blockade valley, i.e. for $\varepsilon = (\varepsilon_{-1,0} + \varepsilon_{0,1})/2 = -U' - \frac{U}{2} = -0.6$, the spin polarization changes sign, as to the right (left) hand side from that point the electron (hole) like virtual processes dominate in the renormalization of the level position.

Note that the abrupt jump of the dot polarization is due to the fact that the underscreened Kondo model is extremely susceptible to even a tiny magnetic field. The reason is that the ground state of the system consists of a Fermi liquid and a decoupled residual spin $S = \frac{1}{2}$ and that residual spin at zero temperature can be polarized by any infinitesimal magnetic field. In the case of a weakly coupled second lead there is a second stage of the Kondo screening at T'_K when the remaining spin degree of freedom is quenched by the weakly coupled lead's electrons.³⁵ In that case the sudden step in the polarization turns into a very steep crossover with a width of $\sim \max(T'_K, T)$, where T is the experimental temperature.

Since the dot spin polarization is rather difficult to detect experimentally, we have computed the level-resolved single particle spectral density $A_{jj'\sigma}(\omega) = -\frac{1}{2\pi} \text{Im} [G_{jj'\sigma}^R(\omega) + G_{j'j\sigma}^R(\omega)]$, where $G_{jj'\sigma}^R(\omega)$ denotes the corresponding retarded Green's function. This quantity contains the information about the transport properties of the dot. Given that the dot is strongly coupled to one of the leads, the conductivity through the setup at voltage bias eV is given by $dI/dV \sim \frac{e^2}{h} \pi \sum_{jj'\sigma} \Gamma_\sigma A_{jj'\sigma}(\omega = eV)$.

The results for the level-resolved normalized spectral functions $\pi\Gamma A_{jj'}^{p=0} = \pi \sum_\sigma \Gamma_\sigma A_{jj'\sigma}^{p=0}$ in the case of nonmagnetic lead ($p = 0$) are shown in Fig. 3. The spectral functions are plotted as a function of energy ω and average level position ε . To resolved the low-energy behavior of spectral functions logarithmic scale for ω is used. Furthermore, only the Coulomb blockade valleys with $N = 1$ and $N = 2$ electrons in the dot are shown. The behavior of spectral functions for blockade valley with $N = 3$ electrons is similar to that with a single electron due to the particle-hole symmetry.

First of all, we note that the two Coulomb blockade regimes with $N = 1$ and $N = 2$ are characterized by fundamentally different fixed points. In the $N = 1$ regime ($-0.2 < \varepsilon < 0.2$) the effective low-energy model is a Fermi liquid with fully screened spin $S = \frac{1}{2}$ ($S = \frac{1}{2}$ Kondo model). On the other hand, in the two-electron regime ($-1 < \varepsilon < -0.2$) the effective model is a singular Fermi liquid,²⁴ i.e. a normal Fermi liquid plus a free spin- $\frac{1}{2}$ with weak residual ferromagnetic coupling to the conduction channel. These two distinct ground states of the system are separated by a quantum phase transition,^{36,37} which occurs when sweeping the gate voltage through the boundary of $N = 1$ ($N = 3$) and $N = 2$ Coulomb valleys. The quantum phase transition is of Kosterlitz-Thouless type,³⁷ with exponentially decreasing Kondo temperature when approaching the transition from the normal Fermi liquid side. The different behavior associated with two distinct fixed points can be

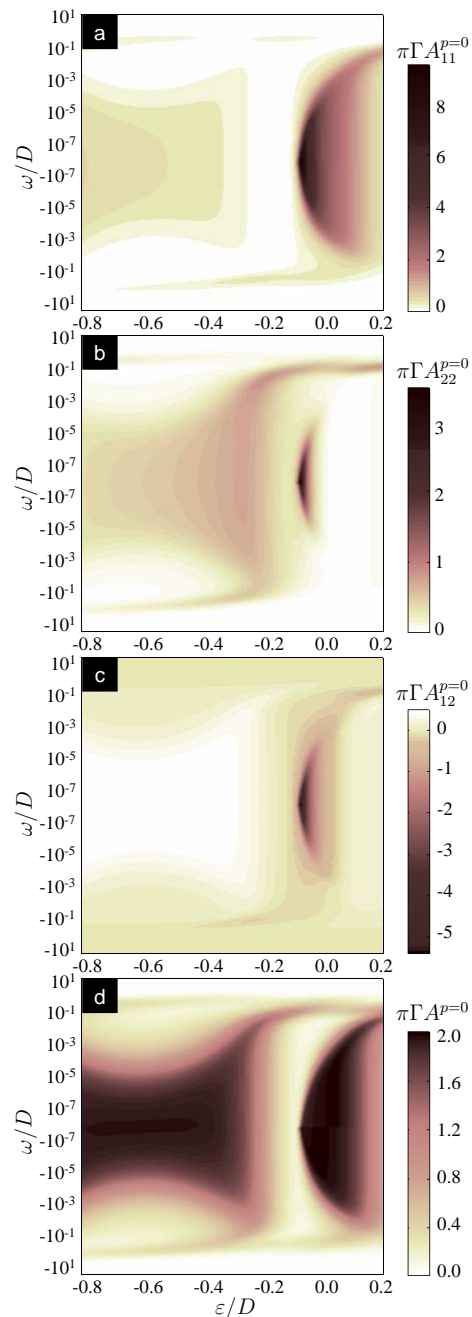


FIG. 3: (color online) The density plots of the normalized level-resolved spectral function $\pi\Gamma A_{jj'}^{p=0} = \pi \sum_\sigma \Gamma_\sigma A_{jj'\sigma}^{p=0}$ (a)-(c) and the full spectral function $\pi\Gamma A^{p=0} = \sum_{jj'} \pi\Gamma A_{jj'}^{p=0}$ (d) in the case when the dot is attached to a nonmagnetic electrode ($p = 0$). The parameters are the same as in Fig. 2 with $\Gamma = 0.04$. Note the logarithmic scale on the frequency axis.

observed in the dependence of the level-resolved spectral functions. In the $N = 1$ Coulomb valley the diagonal elements of the spectral function exceed the unitary value of $\pi\Gamma$, while the off-diagonal elements become negative and their absolute value is also larger than $\pi\Gamma$.

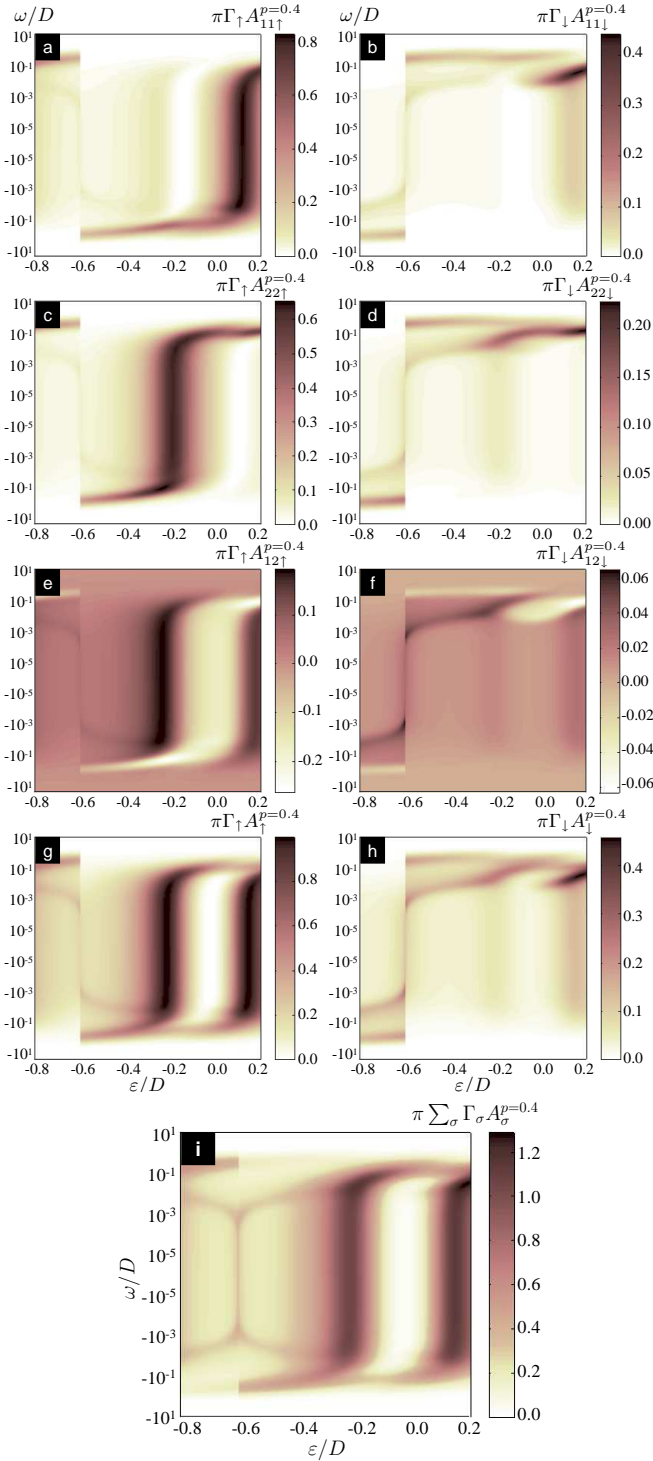


FIG. 4: (color online) The density plots of the spin-dependent level-resolved spectral function $\pi\Gamma_{\sigma}A_{jj'\sigma}^{p=0.4}$ (a)-(f), the spin-dependent full spectral function $\pi\Gamma_{\sigma}A_{\sigma}^{p=0.4} = \sum_{jj'} \pi\Gamma_{jj'\sigma}^{p=0.4}$ (g) and (h), and the full spectral function $\pi\sum_{\sigma}\Gamma_{\sigma}A_{\sigma}^{p=0.4}$ (i) in the case of ferromagnetic lead with $p = 0.4$. The parameters are the same as in Fig. 2 with $\Gamma = 0.04$. Note the logarithmic scale on the frequency axis.

On the other hand, in the $N = 2$ Coulomb blockade

valley, the diagonal and off-diagonal elements of $A^{p=0}$ are rather positive and always smaller than $\pi\Gamma$. In consequence, the full spectral function is properly normalized $A^{p=0} = A_{11}^{p=0} + A_{22}^{p=0} + 2A_{12}^{p=0} = 2\pi\Gamma$ for $\omega = 0$, see Fig. 3(d). Furthermore, the full spectral function clearly exhibits the resonance corresponding to the underscreened Kondo effect in the Coulomb blockade valley $N = 2$ ($\varepsilon < -0.2$), while for $N = 1$ ($\varepsilon > -0.2$) the $S = \frac{1}{2}$ Kondo effect develops.

The spin and level-resolved normalized spectral functions $\pi\Gamma A_{jj'\sigma}^{p=0.4}$ in the case of ferromagnetic lead with $p = 0.4$ are displayed in Fig. 4. Now the spectral function is different for each spin component due to the spin-dependence of the coupling parameters. Furthermore, when the lead is ferromagnetic, both Kondo resonances become completely suppressed. This is directly associated with spin-dependent level renormalization, which lifts the spin degeneracy in the dot, suppressing the spin-flip cotunneling processes driving the Kondo effect. In other words, the ferromagnetic lead exerts an effective exchange field on the dot, which destroys the Kondo effect. There is only a very narrow resonance at $\varepsilon = -0.6$ when the spin splitting of the dot levels generated by the spin imbalance of the conduction electrons vanishes, which happens exactly in the middle of the triplet valley, see also Fig. 2(b).

As mentioned above, the suppression of the Kondo peaks is associated with the exchange field which develops in the presence of spin-dependent couplings. However, as shown in the case of single level quantum dots,^{18,19} one may try to compensate for the presence of the exchange field by applying properly tuned external magnetic field. In Fig. 5 we show the spin-resolved spectral functions calculated in the regime of $S = \frac{1}{2}$ Kondo effect for $\varepsilon = 0$ for different values of magnetic field B . It can be clearly seen that by tuning the magnetic field it is possible to fully restore the Kondo resonance at $\omega = 0$. This happens when $B = B_c = 0.009215$, see Fig. 5, with B_c being the compensating field, i.e. a field at which the previously-split dot level becomes degenerate again.

The situation, however, becomes more complicated for $\varepsilon = -0.4$, which corresponds to the Coulomb valley with $N = 2$ and $S = 1$, when the dot is described by the underscreened Kondo model. The respective spin-resolved spectral functions are shown in Fig. 6 using the logarithmic scale to emphasize the distinct dependence on magnetic field. Because the dot is coupled only to one conduction channel, only a half of the dot's spin can be screened by conduction electrons and the ground state consists of a Fermi liquid and a decoupled spin $S = \frac{1}{2}$. Consequently, at $T = 0$ an infinitesimally small magnetic field is enough to polarize the residual spin-a-half in the dot. This leads to an extremely high sensitivity of transport properties with respect to magnetic field, as can be seen in Fig. 5. In consequence, in order to compensate for the presence of exchange field in the case of underscreened Kondo model, one needs to perform a fine-tuning of magnetic field. Furthermore, it turns out that

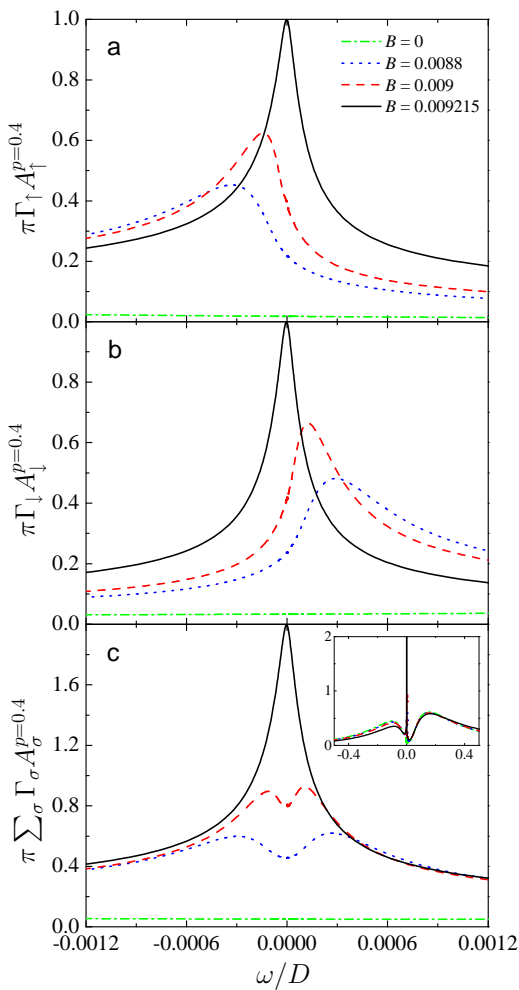


FIG. 5: (color online) The spin-up (a), spin-down (b) and the full (c) spectral function in the $S = \frac{1}{2}$ Kondo regime for $\varepsilon = 0$ in the presence of external magnetic field B , as indicated in the figure. The parameters are the same as in Fig. 2 with $\Gamma = 0.04$ and $p = 0.4$. The inset in (c) shows the zoom-out full spectral function. The Kondo effect is restored when $B = 0.009215$.

although it is possible to restore the resonance peak at $\omega = 0$, the full restoration of the underscreened Kondo effect is not possible, as the height of the peak is below the unitary limit.

IV. CONCLUSIONS

In this paper we have analyzed the equilibrium transport properties of a two-level quantum dot asymmetrically coupled to ferromagnetic leads. We have shown that by tuning the position of the dot levels, the ground state of the system changes from a Fermi liquid in the $S = \frac{1}{2}$ Coulomb valley into a Fermi liquid plus residual spin-a-half in the $S = 1$ Coulomb valley, the latter being the example of underscreened Kondo effect. The boundary between these two regime is a quantum phase tran-

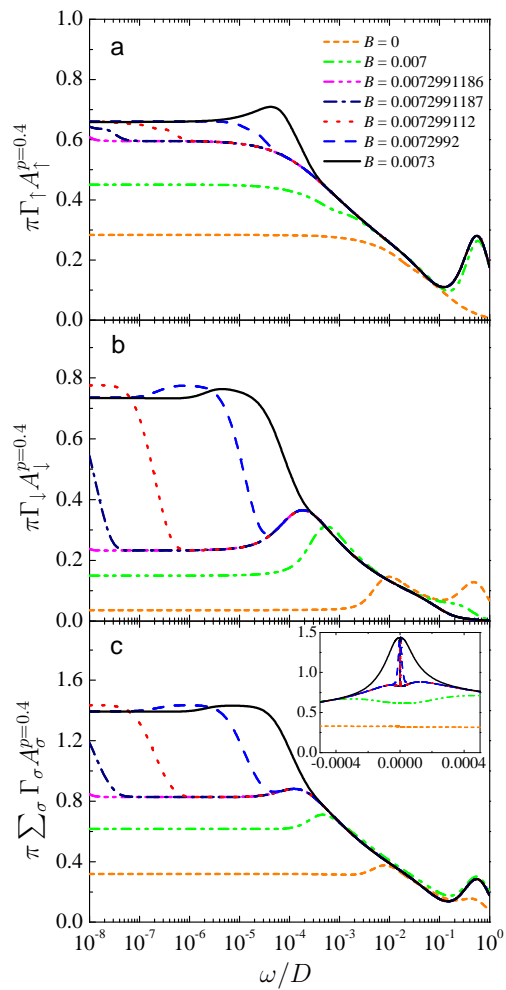


FIG. 6: (color online) The spin-up (a), spin-down (b) and the full (c) spectral function in the underscreened Kondo regime for $\varepsilon = -0.4$ in the presence of external magnetic field B , as indicated in the figure. The parameters are the same as in Fig. 2 with $\Gamma = 0.04$ and $p = 0.4$. The inset in (c) displays the dependence of the spectral function associated with the Kondo peak.

sition. For finite spin polarization of the leads, $p \neq 0$, the Kondo phenomenon becomes suppressed due to an effective exchange field originating from the presence of ferromagnetic leads, and so is the critical behavior.

In the transport regime where the system exhibits underscreened Kondo effect and for $p \neq 0$, we have found that the polarization of the dot abruptly changes sign in the middle of the $S = 1$ Coulomb blockade region. This is associated with virtual tunneling processes (either electron-like or hole-like) that give the dominant contribution to the renormalization of the dot levels.

Furthermore, we have also analyzed the effect of an external magnetic field B applied to the dot. It has been shown that an appropriately tuned B can restore the Kondo effect in the case of the $S = \frac{1}{2}$ Coulomb valley. The underscreened Kondo effect, on the other hand, exhibits an extremely high sensitivity towards even a tiny

change in magnetic field due to its particular ground state. Consequently, an infinitesimally small magnetic field is enough to polarize the residual spin-a-half in the dot, which definitely hinders a full restoration of the underscreened Kondo effect by tuning the magnetic field.

Acknowledgments

We acknowledge fruitful discussions with J. von Delft and R. Žitko. The authors acknowledge support from

the Alexander von Humboldt Foundation. I.W. acknowledges support from the Foundation for Polish Science and funds of the Polish Ministry of Science and Higher Education as research projects for years 2006-2009 and 2008-2010. Financial support by the Excellence Cluster "Nanosystems Initiative Munich (NIM)" is gratefully acknowledged. L.B. acknowledges the support from Hungarian Grants OTKA through projects K73361 and NNF78842.

-
- * Electronic address: weymann@amu.edu.pl
- ¹ W. J. de Haas and G. J. van den Berg, *Physica* **3**, 440 (1936).
 - ² J. Kondo, *Prog. Theor. Phys.* **32**, 37 (1964).
 - ³ A. C. Hewson, *The Kondo Problem to Heavy Fermions* (Cambridge University Press, Cambridge, 1993).
 - ⁴ D. Goldhaber-Gordon, H. Shtrikman, D. Mahalu, D. Abusch-Magder, U. Meirav, and M. A. Kastner, *Nature* (London) **391**, 156 (1998).
 - ⁵ S. Cronenwett, T. H. Oosterkamp, and L. P. Kouwenhoven, *Science* **281**, 182 (1998).
 - ⁶ M. R. Buitelaar, T. Nussbaumer, and C. Schonenberger, *Phys. Rev. Lett.* **89**, 256801 (2002).
 - ⁷ C. Buizert, A. Oiwa, K. Shibata, K. Hirakawa, and S. Tarucha, *Phys. Rev. Lett.* **99**, 136806 (2007).
 - ⁸ A. N. Pasupathy, R. C. Bialczak, J. Martinek, J. E. Grose, L. A. K. Donev, P. L. McEuen, and D. C. Ralph, *Science* **306**, 86 (2004).
 - ⁹ H. B. Heersche, Z. de Groot, J. A. Folk, L. P. Kouwenhoven, H. S. van der Zant, A. A. Houck, J. Labaziewicz, and I. L. Chuang, *Phys. Rev. Lett.* **96**, 017205 (2006).
 - ¹⁰ K. Hamaya, M. Kitabatake, K. Shibata, M. Jung, M. Kawamura, K. Hirakawa, T. Machida, T. Taniyama, S. Ishida and Y. Arakawa, *Appl. Phys. Lett.* **91**, 232105 (2007).
 - ¹¹ K. Hamaya, M. Kitabatake, K. Shibata, M. Jung, M. Kawamura, S. Ishida, T. Taniyama, K. Hirakawa, Y. Arakawa, and T. Machida, *Phys. Rev. B* **77**, 081302(R) (2008).
 - ¹² J. Hauptmann, J. Paaske, P. Lindelof, *Nature Phys.* **4**, 373 (2008).
 - ¹³ H. Yang, S.-H. Yang, S. S. P. Parkin, *Nano Lett.* **8**, 340 (2008).
 - ¹⁴ Rosa Lopez and David Sanchez, *Phys. Rev. Lett.* **90**, 116602 (2003).
 - ¹⁵ J. Martinek, Y. Utsumi, H. Imamura, J. Barnaś, S. Maekawa, J. König, and G. Schön, *Phys. Rev. Lett.* **91**, 127203 (2003).
 - ¹⁶ J. Martinek, M. Sindel, L. Borda, J. Barnaś, J. König, G. Schön, and J. von Delft, *Phys. Rev. Lett.* **91**, 247202 (2003).
 - ¹⁷ Mahn-Soo Choi, David Sanchez, and Rosa Lopez, *Phys. Rev. Lett.* **92**, 056601 (2004).
 - ¹⁸ J. Martinek, M. Sindel, L. Borda, J. Barnaś, R. Bulla, J. König, G. Schön, S. Maekawa, J. von Delft, *Phys. Rev. B* **72**, 121302(R) (2005).
 - ¹⁹ M. Sindel, L. Borda, J. Martinek, R. Bulla, J. König, G. Schön, S. Maekawa, and J. von Delft, *Phys. Rev. B* **76**, 045321 (2007).
 - ²⁰ P. Nozières and A. Blandin, *J. Phys.* **41**, 193 (1980).
 - ²¹ Karyn Le Hur and B. Coqblin, *Phys. Rev. B* **56**, 668 (1997).
 - ²² P. Coleman and C. Pepin, *Phys. Rev. B* **68**, 220405(R) (2003).
 - ²³ A. Posazhennikova and P. Coleman, *Phys. Rev. Lett.* **94**, 036802 (2005).
 - ²⁴ P. Mehta, N. Andrei, P. Coleman, L. Borda, G. Zarand, *Phys. Rev. B* **72**, 014430 (2005).
 - ²⁵ Nicolas Roch, Serge Florens, Theo A. Costi, Wolfgang Wernsdorfer, and Franck Balestro, *Phys. Rev. Lett.* **103**, 197202 (2009).
 - ²⁶ Y. Utsumi, J. Martinek, G. Schön, H. Imamura, and S. Maekawa, *Phys. Rev. B* **71**, 245116 (2005).
 - ²⁷ R. Świrkowicz, M. Wilczyński, M. Wawrzyniak, and J. Barnaś, *Phys. Rev. B* **73**, 193312 (2006).
 - ²⁸ Daisuke Matsubayashi and Mikio Eto, *Phys. Rev. B* **75**, 165319 (2007).
 - ²⁹ P. Simon, P. S. Cornaglia, D. Feinberg, and C. A. Balseiro, *Phys. Rev. B* **75**, 045310 (2007).
 - ³⁰ K. G. Wilson, *Rev. Mod. Phys.* **47**, 773 (1975).
 - ³¹ R. Bulla, T. A. Costi, and T. Pruschke *Rev. Mod. Phys.* **80**, 395 (2008).
 - ³² A. I. Tóth, C. P. Moca, O. Legeza, and G. Zaránd, *Phys. Rev. B* **78**, 245109 (2008).
 - ³³ O. Legeza, C. P. Moca, A. I. Tóth, I. Weymann, G. Zaránd, arXiv:0809.3143 (2008) (unpublished).
 - ³⁴ We used the open access Budapest NRG code, <http://www.phy.bme.hu/~dmnrg/>.
 - ³⁵ A. Posazhennikova, B. Bayani, and P. Coleman, *Phys. Rev. B* **75**, 245329 (2007).
 - ³⁶ M. Pustilnik and L. Borda, *Phys. Rev. B* **73**, 201301(R) (2006).
 - ³⁷ D. E. Logan, Ch. J. Wright, and M. R. Galpin, arXiv:0906.3169 (unpublished).